Journal of Applied Polymer Science

Ultrasonic Decrosslinking of Crosslinked High-Density Polyethylene: Effect of Screw Design

Keyuan Huang, Avraam I. Isayev, Jing Zhong
Department of Polymer Engineering, The University of Akron, Akron, Ohio 44325-0301
Correspondence to: A. I. Isayev (E-mail: aisayev@uakron.edu)

ABSTRACT: The effect of screw design on decrosslinking of the crosslinked high-density polyethylene (XHDPE) by means of ultrasonic twin-screw extruder with two screw configurations is investigated. Die pressure and ultrasonic power consumption during extrusion are recorded. Swelling characteristics, rheological properties, thermal analysis, scanning electron microscopy, and tensile properties are used to investigate the structure–property relationship of decrosslinked XHDPE. It is found that the screw configuration with conveying elements and reverse conveying elements (decrosslinking screws) is an effective means to reduce the gel fraction and crosslink density of decrosslinked XHDPE and significantly improve its processibility. Rheological properties of decrosslinked XHDPE are correlated with structural changes occurring during ultrasonic decrosslinking. The presence of the highly branched sol in decrosslinked XHDPE is revealed through measurements of the activation energy for flow. Comparison of morphologies of the lamellar structure of HDPE, XHDPE, and decrosslinked XHDPE reveals that the presence of the crosslink network inhibits the lamella growth. Significant improvements in the mechanical performance of decrosslinked XHDPE are obtained by using decrosslinking screws. The molecular structure and morphology of the lamellar structure of decrosslinked XHDPE are used to explain the processing–solid-state property relationship. The measured results on the gel fraction and crosslink density are compared with those of numerical simulations. © 2014 Wiley Periodicals, Inc. J. Appl. Polym. Sci. **2014**, *131*, 40680.

KEYWORDS: extrusion; polyolefins; recycling; thermosets

Received 17 January 2014; accepted 6 March 2014
DOI: 10.1002/app.40680

INTRODUCTION

Recycling of crosslinked high-density polyethylene (XHDPE) is a challenge for the plastic industry owing to the presence of the three-dimensional chemical network. An ideal method to reprocess the XHDPE is to preferentially break the crosslinks without breaking the main chains. In case of the silane-crosslinked PE, the crosslinks can be broken without damaging main chains. This is because the Si—O group can be decomposed via methanolysis reaction in the presence of supercritical methanol without degradation of main chains.[1] However, for the peroxide- and irradiation-crosslinked HDPE, the crosslinks and main chains are all C—C bonds. In such cases, the preferential decrosslinking of the peroxide- and irradiation-crosslinked PE is difficult, as reported in a recent study.[2]

The ultrasonic batch reactor and ultrasonic extruder were used to devulcanize various rubber vulcanizate[3,4] and decrosslink XHDPE.[5] The analysis of the gel fraction–crosslink density relationship of ultrasonically devulcanized rubbers showed that the ultrasound induced a preferential breakage of crosslinks.[6] In recent study,[7] decrosslinking of XHDPE via the ultrasonic single-screw extruder (SSE) and twin-screw extruder (TSE) was reported indicating that both the mechanical shearing and ultrasound cause decrosslinking. By varying processing conditions, the lowest gel fraction of about 0.5 for the decrosslinked XHDPE was obtained from TSE. The mechanical performance of the decrosslinked XHDPE from TSE containing the kneading elements was shown to be inferior to that from SSE and the virgin XHDPE. It seems that the screws containing the kneading elements cause a substantial degradation of polymer chains during decrosslinking of XHDPE. To reduce degradation and improve the performance of the ultrasonically decrosslinked XHDPE, an improvement of the screw configuration is necessary.

This study is aimed to modify TSE screw design to improve ultrasonic decrosslinking of XHDPE. In particular, the effect of two different screw designs on the ultrasonic decrosslinking is investigated and rheological, mechanical, and structural properties of the decrosslinked XHDPE are compared. In addition, the evolution of the gel fraction and crosslink density in the ultrasonic decrosslinking process was simulated based on a simplified theoretical model describing the ultrasonic devulcanization

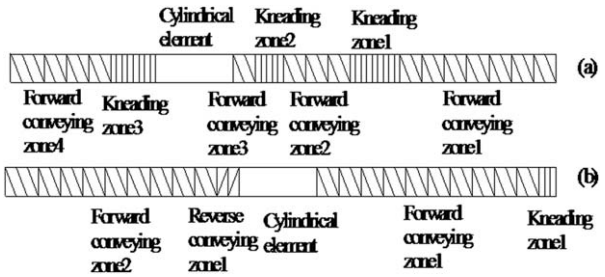

Figure 1. Schematics of the compounding (a) and decrosslinking (b) screws. The flow direction is from right to left.

of rubbers.[6,8] The predicted results are compared with the corresponding experimental data.

EXPERIMENTAL

Materials

HDPE used was a rotational molding grade, 35 mesh powder (Paxon 7004, Exxon Mobil, Baytown, TX). Crosslinking agent was dicumyl peroxide in the pellet form (DC-40, Akrochem, Akron, OH). It contains 40 wt % peroxide and 60 wt % calcium carbonate as a carrier. Tetrakis[methylene(3,5-di-*tert*-butyl-4-hydroxyhydrocinnamate)] methane (Antioxidant 1010, Akrochem) was used as a stabilizer during the rheology test. Xylene (mixture of isomers, ACS Reagent Grade, Sigma-Aldrich, WI) was used as a solvent for the swelling test. Hexane (ACS Reagent Grade, J.T. Baker, Pittsburgh, PA) was used to precipitate the dissolved sol from xylene. The sol was the soluble fraction of samples in the swelling test. The concentration of active peroxide in the crosslinking recipe was 1 wt %, which is a typical crosslinking recipe for the rotational molded XHDPE.[9] Details of preparation of XHDPE can be found elsewhere.[7]

Decrosslinking of XHDPE via Ultrasonic Twin-Screw Extrusion

Decrosslinking was carried out using an ultrasonic 16-mm corotating TSE (PRISM US LAB 16, L/D = 24, Thermo Electron Corporation, MA) equipped with a circular die with a diameter of 3 mm and a length of 11 mm. A water-cooled ultrasonic horn with a power of 800 W operating at 40 kHz (Branson 2000 bdc, Branson Ultrasonic, CT) was used providing the longitudinal ultrasonic wave orthogonal to the flow direction. The barrel and die temperature was set up at 200°C. The flow rate was maintained at 6.5 g/min corresponding to a mean residence time of 17.5 s in the ultrasonic treatment zone. The ultrasonic amplitudes were 5, 7.5, 10, and 13 μm. The die pressure and ultrasonic power consumption were recorded. All other procedures and equipment were same as those in the previous study.[7] It should be noted that no noticeable damage on the horn surface was seen by the ultrasonic treatment as the horn was made of a titanium alloy and cooled by water.

Screw Design

Figure 1 shows schematics of two sets of screw design used. The first design [Figure 1(a)] was a typical compounding screw design containing kneading elements and forward conveying elements and called compounding screws. The cylindrical elements in the screws were used to provide a uniform gap of 2.54 mm between the screw and the ultrasonic horn surface in the ultrasonic treatment zone. The second design [Figure 1(b)] was an improved screw design for the purpose of decrosslinking and called decrosslinking screws. To minimize the mechanical degradation of XHDPE generated by kneading elements of the first design, they were replaced by the conveying elements. Also, two reverse conveying elements were placed next to the cylindrical elements in the downstream section. The purpose of the reverse elements is to ensure a complete filling of the gap between the ultrasonic horn and the screw. It should be noted that three kneading elements were placed at the feed section of the decrosslinking screws to appropriately position the cylindrical elements. As the material was fed at the second forward conveying element, the kneading elements in the decrosslinking screws had no effect on the extrusion of XHDPE.

Preparation of Specimens and Their Characterization

The compression molded sheets of XHDPE and decrosslinked XHDPE were prepared by following the same procedure as in Ref. 7. The sheets were molded at a temperature of 200°C and a pressure of 50 MPa for 20 min.

Swelling of XHDPE and decrosslinked XHDPE was performed by following ASTM D 2765, test method C except for the decrosslinked XHDPE obtained at an ultrasonic amplitude of 13 μm. At this amplitude the crosslink density of the sample was too low causing its disintegration after swelling for 24 h. Thus, the gel fraction of this decrosslinked XHDPE was determined according to the ASTM D 2765, test method A with a small modification. Specifically, a razor sliced sample of a size about 0.01 mm^3 instead of 30-mesh ground sample was used. The sliced sample of about 0.15 g was sealed into a cage made of 120-mesh stainless steel cloth. The cage was kept in boiling xylene for 24 h to dissolve soluble fraction (sol) completely. The gel fraction of the XHDPE and decrosslinked XHDPE was taken as the ratio of weights of the original sample to dried swollen sample. The crosslink density of the XHDPE and decrosslinked XHDPE was determined by Flory–Rehner equation.[10] Consistency of the measurement of the gel fraction by two different methods was within 3%.

Small amplitude oscillatory shear (SAOS) test of the XHDPE and decrosslinked XHDPE at a temperature of 160°C was performed by using a stress-controlled Discover Hybrid Rheometer (DHR-2, TA Instruments, New Castle, DE) equipped with 25-mm parallel plates. A circular disk of a diameter of 25 mm was cut from the compression molded sheet. A gap of 2 mm was used for the test. By measuring dynamic properties at different gaps (2 and 1.5 mm), it was proven that no slippage occurred during the test.[11] The frequency sweep was in the range from 0.1 to 100 rad/s at the stress amplitude of 500 Pa during SAOS. It was confirmed that this stress amplitude is within the linear region. SAOS test of the HDPE, sol of the XHDPE, and decrosslinked XHDPE at temperatures of 140, 150, and 160°C was also performed to calculate the activation energy for flow. Because of the limited amount of sol, a 25-mm circular disk of a thickness of 0.4 mm was used. For various sols and virgin HDPE, the frequency sweep was in the range from 0.5 to 79

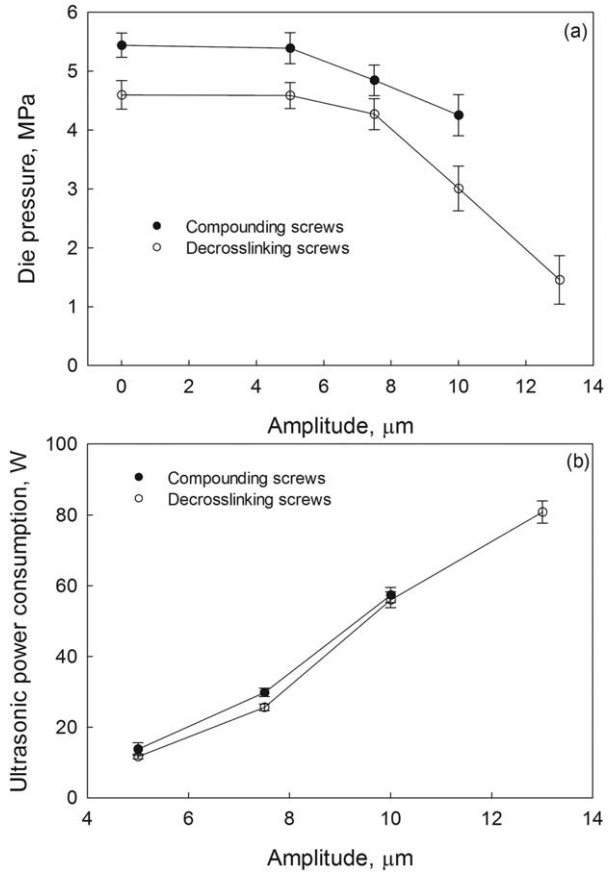

Figure 2. Die pressure (a) and ultrasonic power consumption (b) as a function of the ultrasonic amplitude during extrusion of XHDPE for TSE containing compounding (filled symbols) and decrosslinking (open symbols) screws.

rad/s at the stress amplitude of 250 Pa. All the SAOS were repeated twice with the difference being less than 3%.

Differential scanning calorimetry (DSC, Model Q200, TA Instruments) was used to investigate the thermal behavior of the HDPE, XHDPE, and decrosslinked XHDPE. Samples were cut from tensile specimens by a stainless steel one-sided razor blade. The samples of about 10 mg were sealed into the DSC hermetic pans (PS 1007, PS 1010, Instrument Specialist, Twin Lakes, WI). To remove the thermal history, the heating-cooling-heating cycle at a rate of 10°C/min was applied. Samples were heated from 40 to 200°C, then maintained at 200°C for 10 min, cooled from 200 to 40°C and equilibrated at 40°C, and finally heated from 40 to 200°C. The melting temperature and enthalpy were calculated from the second heating. The melting enthalpy of 282 J/mol of the perfect linear PE crystal[12] was used to evaluate the crystallinity. The reported crystallinity and melting temperature are the average value of at least two measurements.

A field-emission scanning electron microscope (JEOL-7401, Japan Electron Optics Laboratory, Japan) was used to observe the morphology of the crystalline structure of the virgin HDPE, XHDPE, and decrosslinked XHDPE. The samples were cryofractured in liquid nitrogen. To remove the amorphous phase the cryofractured surface was etched by a mixture of 1 vol H_2SO_4 : 1 vol H_3PO_4 and 1 wt % $KMnO_4$.[13] The etching time was varied to avoid destruction of the lamellar structure. An acceleration voltage of 1.0 or 2.0 kV was used. The sample was mounted on the aluminum stub. A sputter coater (K575X, Quorum Technologies, UK) was used to coat the surface with silver to provide the conductivity.

Tensile test was performed by using an Instron tensile tester (Mode 5567, Instron, MA) at a crosshead speed of 25 mm/min without an extensometer. Dumbbell-shaped tensile specimens were cut from the compression molded sheet by using a cutting die of a width of 5 mm and a gauge length of 23 mm. The stress–strain curves were recorded by a PC and used to calculate the Young's modulus, yield stress, and stress and strain at break. The error bars were calculated as the standard deviation of at least five test results.

RESULTS AND DISCUSSION

Die Pressure and Ultrasonic Power Consumption

Figure 2 shows the die pressure (a) and ultrasonic power consumption (b) as a function of the ultrasonic amplitude during the extrusion of XHDPE at a flow rate of 6.5 g/min for TSE using two different screw configurations. It is seen that the die pressure decreases with the amplitude. The decrease of the die pressure is the result of a reduction of viscosity and therefore an improvement of the processibility due to a decrease of the gel fraction and crosslink density with the amplitude. At the same amplitude the die pressure in TSE containing the decrosslinking screws is lower than that in TSE containing the compounding screws. As shown below, the former TSE is more effective in reducing the gel fraction and crosslink density of the decrosslinked XHDPE in comparison with the latter TSE.

It is seen from Figure 2(b) that the ultrasonic power consumption is only slightly affected by screw configurations and increases with the ultrasonic amplitude owing to an increase of the acoustic pressure. The ultrasonic power consumption is proportional to the acoustic pressure.[8] It is noteworthy to point out that the ultrasonic power consumption alone should not be considered as a measure of the effect of ultrasonic treatment on the material structure, e.g., gel fraction and crosslink density. In fact, according to the simulation study,[6] the change of the gel fraction and crosslink density is also determined by the bubble volume fraction and intensity of bubble dynamics induced by the ultrasound.

Gel Fraction and Crosslink Density

Figure 3 shows the gel fraction (a) and crosslink density (b) of the decrosslinked XHDPE as a function of the ultrasonic amplitude from TSE containing different screws. The gel fraction and crosslink density of the XHDPE are also indicated. It can be seen that the gel fraction and crosslink density of the decrosslinked XHDPE are significantly reduced even when the XHDPE passed through the extruder without being treated by ultrasound.

The rupture of the crosslink network of a crosslinked PDMS as a model network upon imposition of the large step shear strain was studied in Ref. 14. An important conclusion drawn from the study is that the extent of the network rupture is determined by the magnitude of strain experienced by the polymer.

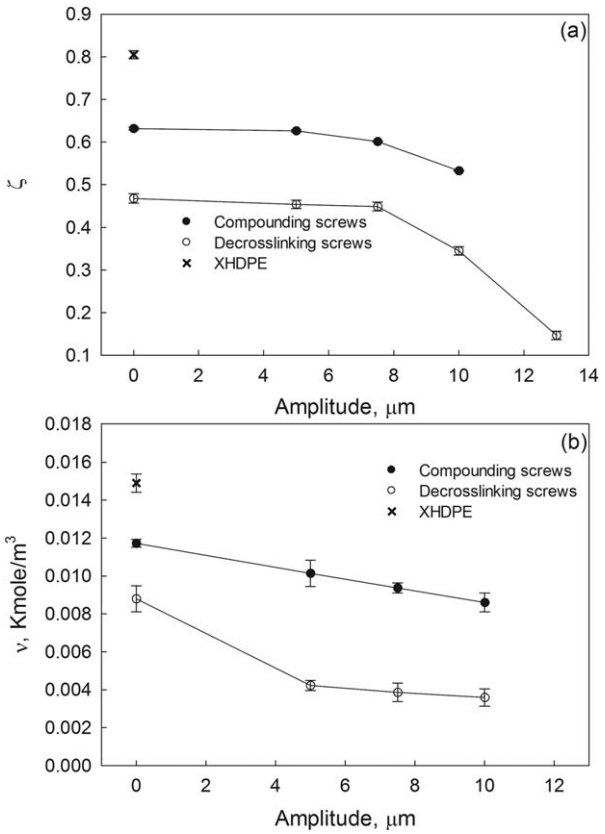

Figure 3. Gel fraction (a) and crosslink density (b) of the decrosslinked XHDPE as a function of the ultrasonic amplitude from TSE containing compounding (a) and decrosslinking (b) screws. Values for XHDPE are also indicated.

The reason for the mechanical rupture of the crosslinked PDMS is due to the finite extensibility of polymer chains in a crosslink network. Also, a model describing the network rupture subjected to the ultrasound was proposed in Ref. 6. According to this model, the gel fraction and crosslink density can be substantially reduced. In case of TSE, a substantial strain is experienced by the XHDPE in the kneading mixing zone and the gap between the ultrasonic horn and rotating shafts. It is surprising to see that the gel fraction of the decrosslinked XHDPE without any ultrasonic treatment from TSE containing decrosslinking screws is lower than that from TSE containing the compounding screws. Considering the presence of kneading elements in the compounding screws and their absence in the decrosslinking screws, it is natural to suggest that the compounding screws are more effective in applying large strains on the XHDPE than the decrosslinking screws. However, it should be noted that such a statement is valid only in the absence of wall slip of the XHDPE along the barrel and screw surfaces. Evidently, the no-slip condition does not hold for the XHDPE owing to its high gel fraction. Therefore, the strain applied on the XHDPE is affected by the slip velocity. Obviously, the strain should increase as the slip velocity decreases. The slip velocity of the molten polymer is known to decrease with an increase of pressure.[15] The reverse conveying elements in the decrosslinking screws can generate a higher pressure than the reverse kneading elements in the compounding screws. Therefore, a higher pressure can be achieved in the gap between the barrel and rotating shafts in the TSE containing the decrosslinking screws than in TSE containing the compounding screws. Thus, the decrosslinking screws can apply a larger strain on the XHDPE than the compounding screws, yielding a lower gel fraction and crosslink density of the decrosslinked XHDPE by mechanical shearing alone.

Also, it is seen in Figure 3 that the gel fraction and crosslink density of the decrosslinked XHDPE decrease with the ultrasonic amplitude. A more decrosslinking is achieved at an amplitude of 13 μm in TSE containing decrosslinking screws yielding the decrosslinked XHDPE with a gel fraction of 15%. According to the simulation,[16] an increase of the ultrasonic amplitude leads to an increase of bubble volume fraction and intensity of bubble dynamics. This may lead to a more decrease of the gel fraction and crosslink density of the decrosslinked XHDPE. From Figure 3, it is also seen that when the ultrasound is applied, TSE containing the decrosslinking screws is more effective in decreasing both the gel fraction and crosslink density of the decrosslinked XHDPE than TSE containing the compounding screws. Strictly speaking, owing to the superposition of the mechanical and ultrasonic decrosslinking of XHDPE, it is impossible to separate the effect of ultrasound on the gel fraction and crosslink density. Obviously, there is an interaction between two different decrosslinking processes. However, one can simplify the situation by neglecting such an interaction by considering the mechanical and ultrasonic decrosslinking processes being independent. With this assumption it is possible to determine the ultrasonic effect on the gel fraction and crosslink density of the decrosslinked XHDPE as:

$$\Delta\zeta_{\text{ultra}} = \zeta_{\text{nonultra}} - \zeta_{\text{mech+ultra}} \quad (1)$$

$$\Delta\nu_{\text{ultra}} = \nu_{\text{nonultra}} - \nu_{\text{mech+ultra}} \quad (2)$$

where $\Delta\zeta_{\text{ultra}}$ and $\Delta\nu_{\text{ultra}}$ are, respectively, the change of the gel fraction and crosslink density of the decrosslinked XHDPE due to the ultrasonic treatment alone, ζ_{nonultra} and $\Delta\nu_{\text{nonultra}}$ are, respectively, the gel fraction and crosslink density of the decrosslinked XHDPE due to mechanical decrosslinking only, $\zeta_{\text{mech+ultra}}$ and $\nu_{\text{mech+ultra}}$ are, respectively, the gel fraction and crosslink density of the decrosslinked XHDPE due to mechanical and ultrasonic decrosslinking. It is seen from Figure 3 that at high ultrasonic amplitudes the treatment is more effective in the TSE containing the decrosslinking screws than in the TSE containing the compounding screws. For example, at an amplitude of 10 μm, $\Delta\zeta_{\text{ultra}} = 0.12$ and $\Delta\nu_{\text{ultra}} = 5.2 \times 10^{-3}$ kmol/m^3 for the decrosslinked XHDPE from the former TSE, whereas at this amplitude $\Delta\zeta_{\text{ultra}} = 0.10$ and $\Delta\nu_{\text{ultra}} = 3.1 \times 10^{-3}$ kmol/m^3 for the decrosslinked XHDPE from the latter TSE.

The ultrasonic decrosslinking of XHDPE is affected by many factors including acoustic properties of the polymer, hydrostatic pressure in the ultrasonic treatment zone, ultrasonic amplitude, residence time, and gel fraction and crosslink density. To understand what causes the significant differences between the decrosslinking and compounding screws on the ultrasonic decrosslinking of the XHDPE at an amplitude of 10 μm, simulations of the effect of hydrostatic pressure and gel fraction of the polymer entering the ultrasonic treatment zone were performed. The simulation program is developed based on a

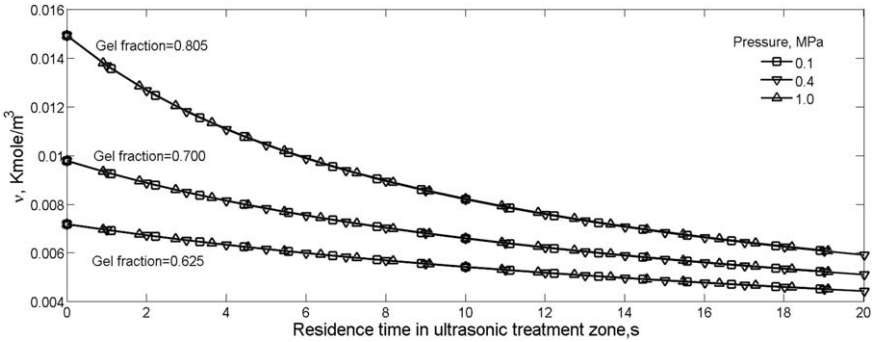

Figure 4. Simulated crosslink density of decrosslinked XHDPE containing different initial gel fractions as a function of the residence time at an ultrasonic amplitude of 10 μm and different hydrostatic pressures.

simplified model describing the ultrasonic devulcanization of rubbers.[6] This model is suitable to compute the gel fraction and crosslink density of ultrasonically devulcanized rubber using the hydrostatic pressure and crosslink density of the virgin rubbers as input parameters. As the model[6] did not incorporate the effect of the residence time, it is modified in this study (see Appendix).

As the pressure in the ultrasonic treatment zone cannot be directly measured, it is approximated from the pressure recorded by a transducer placed before the ultrasonic treatment zone indicating 0.32 and 0.05 MPa, respectively, in TSE containing the compounding screws and decrosslinking screws. To evaluate the effect of the pressure on the ultrasonic decrosslinking of XHDPE, hydrostatic pressures of 0.1, 0.4, and 1 MPa were used in simulations at gel fractions of the material entering the ultrasonic treatment zone being 0.805, 0.7, and 0.625. It is believed that the range of the hydrostatic pressure covers the pressure in the ultrasonic treatment zone during the ultrasonic decrosslinking. Figure 4 shows the simulated crosslink density of the decrosslinked XHDPE as a function of the residence time during the ultrasonic treatment. It is seen from Figure 4 that the effect of hydrostatic pressure on the crosslink density is insignificant with difference being less than 3% when pressure is increased from 0.1 to 1 MPa. Thus, a hydrostatic pressure of 0.4 MPa is used for further simulation.

Figure 5 shows the simulated reduction of the gel fraction (a) and crosslink density (b) of the decrosslinked XHDPE as a function of the residence time in the ultrasonic treatment zone caused by the ultrasonic treatment alone in TSE containing the compounding and decrosslinking screws. The corresponding measured reductions of these quantities for the decrosslinked XHDPE at a residence time of 17.5 s are also indicated. As seen from Figure 5, both the simulations and measurements indicate that the ultrasonic treatment is more effective in case of the network of higher gel fraction and higher crosslink density. Clearly, a larger decrease of the gel fraction and crosslink density occurs at higher gel fraction and crosslink density. A good agreement between the simulated and measured reduction for the crosslink density is obtained when the gel fraction of the material entering the ultrasonic zone in TSE containing the compounding and decrosslinking screws is taken 0.65 and 0.725, respectively. However, there is a discrepancy between the simulated and measured reduction of the gel fraction, as seen from Figure 5(a). The reason for the discrepancy is mainly due to the fact that the employed model assumes only main-chain breakage during decrosslinking. This assumption leads to an overestimation of the reduction of the gel fraction for decrosslinking of XHDPE. As shown in Ref. 6, a higher decrease of the gel fraction occurs in case of the main-chain scission than that of the crosslink scission.

Rheology

Figure 6 shows the storage (a), loss moduli (b), complex viscosity (c), and loss tangent (d) of XHDPE and decrosslinked XHDPE from TSE containing the compounding and decrosslinking screws without and with ultrasonic treatment at various ultrasonic amplitudes as a function of the frequency at a temperature of 160°C. It is seen in Figure 6(a–c) that in double logarithmic scale the storage and loss moduli and complex viscosity of the XHDPE and decrosslinked XHDPE are linearly dependent on the frequency. As seen in Figure 6(d), the loss tangent of the XHDPE exhibits the weak frequency dependence with a slight increase above a frequency of 10 rad/s. In contrast, the loss tangent of the decrosslinked XHDPE slightly decreases with the frequency. As the highest storage modulus is lower than the plateau modulus, G_N^0, of PE, the frequency range used is below the rubbery plateau. Dependences of the storage and loss moduli and, therefore, the complex viscosity of the crosslinked PE in the vicinity of its gel point below the rubbery plateau are described by a scaling law[17]:

$$G' \propto \omega^m \tag{3}$$

$$G'' \propto \omega^m \tag{4}$$

$$|\eta^*| = K\omega^n \tag{5}$$

where ω is the angular frequency, m and n is the power-law index, and K is the consistency. The power-law behavior of the storage modulus and complex viscosity in the frequency range below the rubbery plateau is the characteristics of a polymer near its gelation point of a lightly crosslinked polymer.[17–21] The average molecular weight between crosslinks (M_c) in the XHDPE is determined as follows:

$$M_c = \frac{\rho}{v} \tag{6}$$

where ρ is the density and v is the crosslink density. According to eq. (6), the value of M_c of XHDPE is 5.4×10^4 g/mol. The

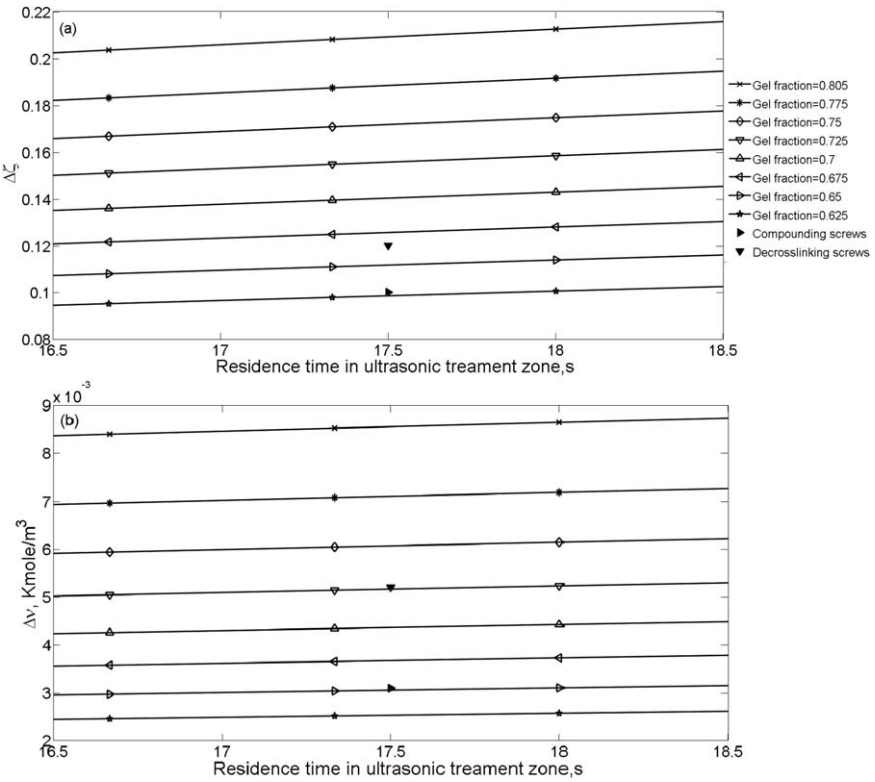

Figure 5. Simulated changes in values of the gel fraction (a) and crosslink density (b) of XHDPE due to ultrasonic treatment alone as a function of the residence time at an ultrasonic amplitude of 10 μm in TSE containing compounding and decrosslinking screws. The corresponding measured values are also indicated.

dependence of the zero-frequency viscosity on M_w of the HDPE at 150°C is given in Ref. 22 as

$$\eta_o = 9.0 \times 10^{-15} (M_w)^{3.6} \tag{7}$$

Based on the measured value of η_o [see Figure 7(a)] and eq. (7), M_w of the virgin HDPE is 5.17 $\times$ 10^4 g/mol, which is close to the M_c of XHDPE. This indicates that the XHDPE indeed is a lightly crosslinked polymer ($M_w \approx M_c$) and, therefore, the decrosslinked XHDPE is also lightly crosslinked polymers with their rheological behavior described by eqs. (3–5).

It is seen from Figure 6 that the decrosslinked XHDPE exhibits a lower storage modulus and complex viscosity but a higher loss tangent compared to those of the XHDPE with the effect being stronger at higher ultrasonic amplitudes. At the same amplitude the decrosslinked XHDPE from TSE containing the decrosslinking screws exhibits a lower storage modulus and complex viscosity and higher loss tangent. Although the dependence of the loss modulus of the decrosslinked XHDPE on the ultrasonic amplitude and screw configuration is more complex, as shown in Figure 6(b), the dependence of other rheological properties on these parameters is correlated with that of the gel fraction and crosslink density. This is due to the fact that the rheological behavior of a crosslinked polymer in the low frequency region is mainly governed by its crosslinked network. Earlier studies on the crosslinked HDPE,[20] crosslinked low-density PE (LDPE),[21] and crosslinked linear ethylene-butene copolymer[18] suggested that the complex viscosity and storage modulus of the crosslinked PE increase with the gel fraction and crosslink density. Also, a decrease of the loss tangent with the gel fraction and crosslink density is seen in these studies. Thus, the dependence of the rheological behavior of the decrosslinked XHDPE on processing conditions and screw configurations during extrusion can be correlated with structural changes.

The XHDPE and decrosslinked XHDPE comprise the gel and sol. Thus, their physical properties are not only influenced by their gel fraction and crosslink density but also by the molecular structure of the sol. As the rheological properties of PE are very sensitive to the molecular structure,[23–27] dynamic properties of sols at various temperatures shall reveal such information. Figures 7 and 8 show the complex viscosity of the HDPE and sols of the XHDPE and decrosslinked XHDPE obtained at various processing conditions as a function of the frequency at various temperatures. Cross model[28] fit is also indicated in Figures 7 and 8. The following two equations are used for this fitting:

$$|\eta^*| = \frac{\eta_o^*(T)}{1 + \left[\frac{\eta_o^*(T)\varpi}{\tau}\right]^{1-n}} \tag{8}$$

$$\eta_o^*(T) = A\exp\left(\frac{T_b}{T}\right) = A\exp\left(\frac{E}{RT}\right) \tag{9}$$

where A, T_b, τ, and n are fitting parameters. The function of $\eta_o^*(T)$ is the temperature dependency of the zero-frequency viscosity by the Arrhenius equation, where T is the temperature, E is the activation energy for flow, and R is the gas constant.

The activation energy for flow of the entangled PE depends on its chain branching.[23–27,29] As HDPE and sols of XHDPE and

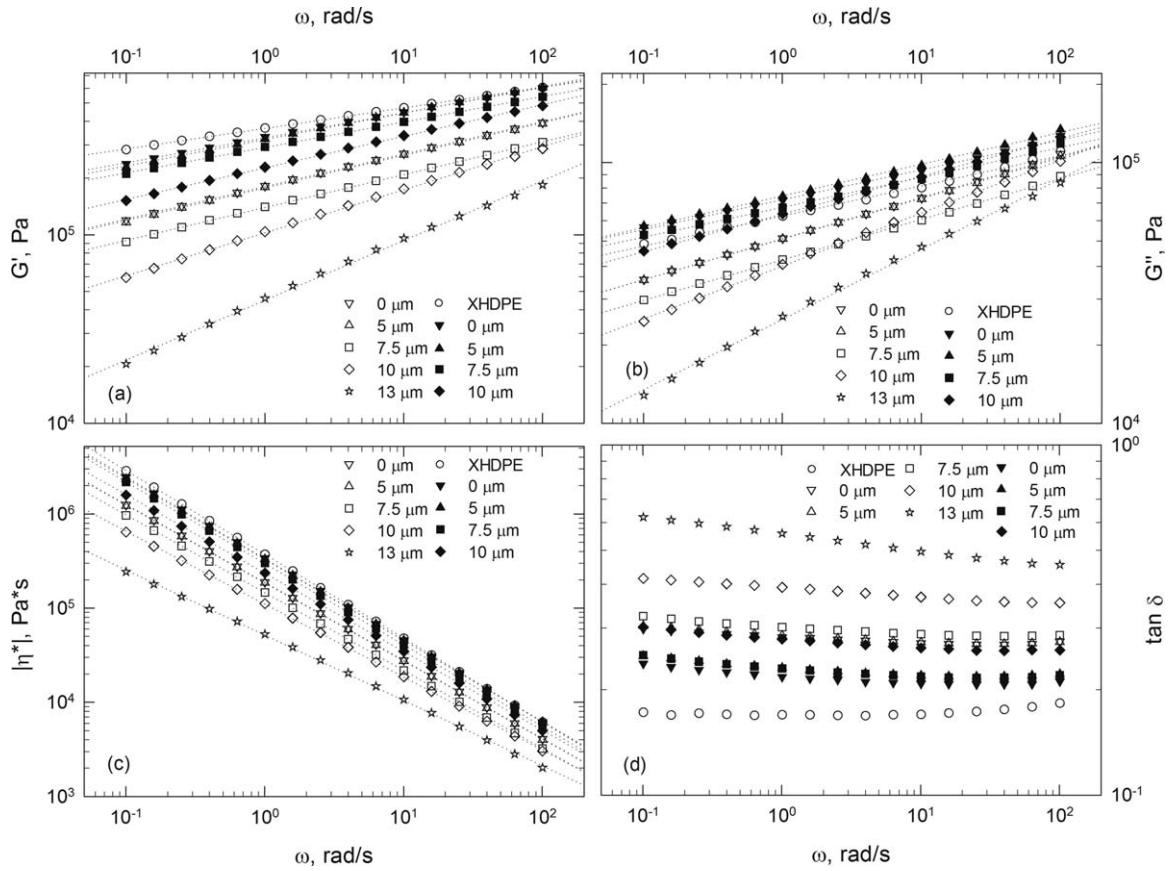

Figure 6. Frequency dependence of storage (a) and loss moduli (b), complex viscosity (c), and loss tangent (d) of XHDPE and decrosslinked XHDPE without ultrasonic treatment and with ultrasonic treatment at various ultrasonic amplitudes from the TSE containing compounding screws (filled symbols) and decrosslinking screws (open symbols). Dotted lines represent power-law model fits, eqs. (3)–(5), respectively.

decrosslinked XHDPE are well entangled, values of the activation energy for flow of HDPE and various sols of decrosslinked XHDPE are affected by chain branching. It can be seen from Table I that the activation energy of HDPE, owing to its linear molecular structure, is lowest among all the studied samples. The activation energy of sols of XHDPE and decrosslinked XHDPE is higher than that of HDPE. Therefore, sols are branched PEs. The chain branching in the sol of XHDPE is certainly not inherited from HDPE, but generated during its crosslinking. HDPE melt is crosslinked by the radicals with the interlink reaction between PE molecules taking place before the gel formation. The chain branching is certainly generated during the reaction, unless two chains having radicals at chain ends combine together. As peroxide crosslinking of HDPE is a statistical random process, the probability of two chains with radicals at chain ends combine together is very low. Thus, the chain branching in the sol of XHDPE is caused by the statistical randomness of the interlink reaction initiated by peroxide radicals.

The value of the activation energy of the sol of decrosslinked XHDPE is close to that of commercial LDPE,[29] suggesting the occurrence of a long-chain branching. The long-chain branching in the sol of decrosslinked XHDPE is a result of the main-chain scission during decrosslinking of XHDPE. If one assumes that the main-chain scission in XHDPE takes place in the middle of the polymer chain between crosslinks, the molecular weight of branches generated by this chain scission will be half of M_c, which is equal to 2.7×10^4 g/mol. The molecular weight of branches is by one order of the magnitude higher than the entanglement molecular weight, M_e, of PE. Therefore, decrosslinking leads to the long-chain branching. As chemical bonds in polymer chains and crosslinks in XHDPE are identical, its main-chain scission is inevitable.

The molecular structure of various sols can be further inferred through comparison of the complex viscosity dependence of HDPE and sols on the frequency. HDPE exhibits a terminal behavior with a Newtonian viscosity region [see Figure 7(a)]. The complex viscosity of the sol of XHDPE is lower than that of HDPE. This is because this sol is the product of the interlink reaction of the low molecular fraction of HDPE. During HDPE crosslinking, longer chains are incorporated into the gel network earlier than the shorter chains. Thus, M_w of XHDPE sol is lower than that of HDPE resulting in a lower complex viscosity. It can be seen from Figure 7(c–f) and Figure 8(a–e) that the complex viscosity of various sols of the decrosslinked XHDPE is higher than that of HDPE and sol of XHDPE. A strong non-Newtonian behavior of the complex viscosity of sols of the decrosslinked XHDPE is seen. This is caused by the presence of

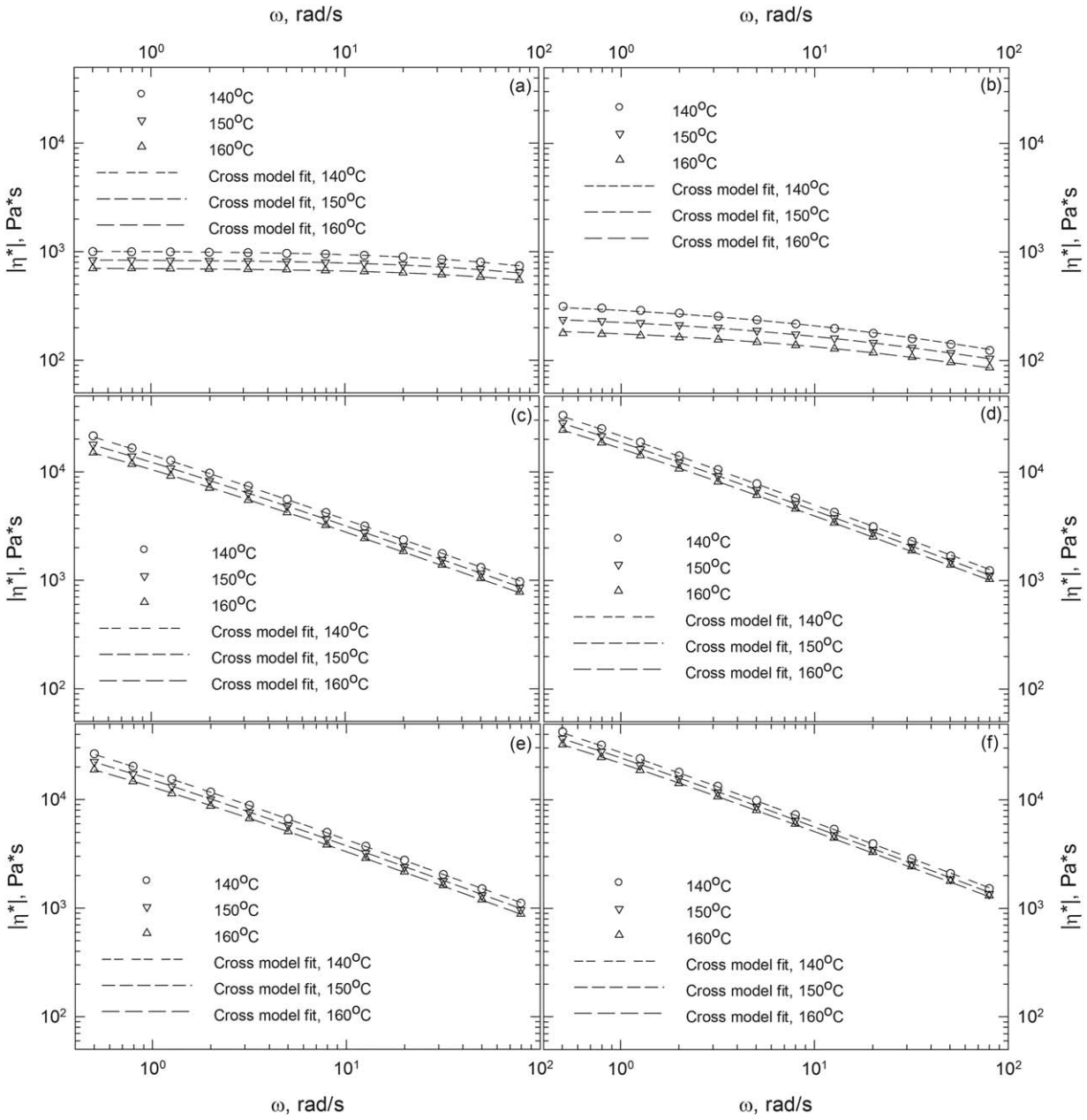

Figure 7. Frequency dependence of complex viscosity of HDPE (a), sols of virgin XHDPE (b), and decrosslinked XHDPE from TSE containing compounding screws without ultrasonic treatment (c) and with ultrasonic treatment at ultrasonic amplitudes of 5 μm (d), 7.5 μm (e), and 10 μm (f). Dashed lines represent cross model fits, eqs. (8) and (9).

the long-chain branching in sols and their high molecular weight. Despite differences in the complex viscosity of sols of the decrosslinked XHDPE obtained from TSE containing different screws at various processing conditions, sols exhibit similar molecular structures, i.e., sols are highly branched PEs with the long-chain branching. The dependence of the complex viscosity of sols of the decrosslinked XHDPE on the processing conditions and screw configurations is very complicated. It is known that rheological behavior of PE is very sensitive to the chain topology including the length of the main chains and branches as well as the distribution of chain branching.[23–27] As the relation between the chain topology of sols of the decrosslinked XHDPE and processing conditions is not clear, it is impossible to further identify the dependence of rheological behavior of sols on these conditions.

DSC Analysis

Figure 9 shows the crystallinity (a) and melting temperature (b) of the decrosslinked XHDPE as a function of the ultrasonic amplitude. For comparative purposes these values for the HDPE and XHDPE are also given in this figure. It is seen that HDPE owing to its linear molecular structure exhibits the highest crystallinity and melting temperature. Also, the crystallinity and melting temperature of XHDPE are lower than those of

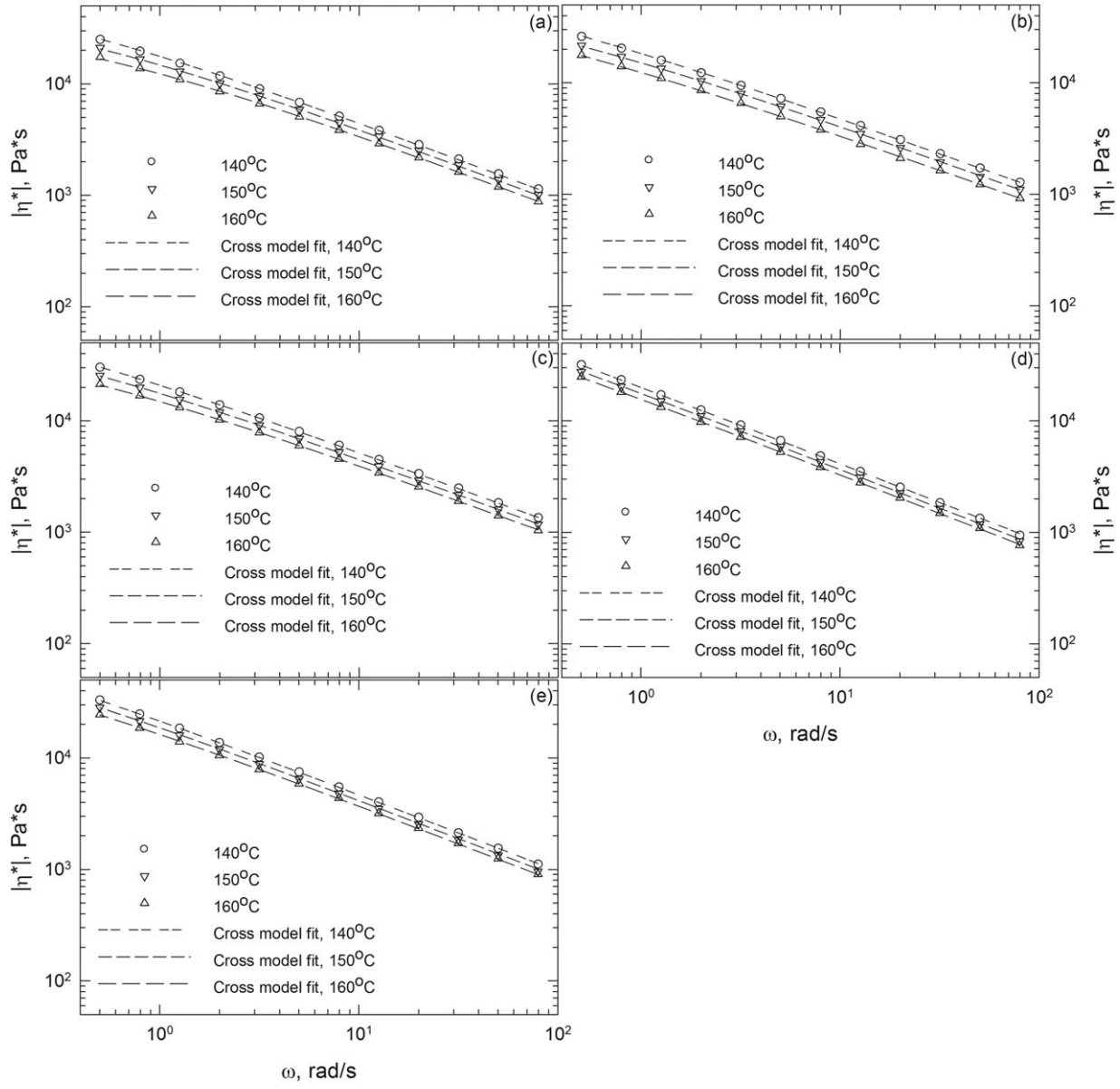

Figure 8. Frequency dependence of complex viscosity of sols of decrosslinked XHDPE from TSE containing decrosslinking screws without ultrasonic treatment (a) and with ultrasonic treatment at ultrasonic amplitudes of 5 μm (b), 7.5 μm (c), 10 μm (d), and 13 μm (e). Dashed lines represent cross model fits, eqs. (8) and (9).

HDPE. This is due to the presence of the crosslink network and branched sol of XHDPE. The crystallinity of the decrosslinked XHDPE from TSE containing the compounding and decrosslinking screws is, respectively, lower and higher than that of XHDPE while the melting temperature is lower, except for the sample obtained without ultrasonic treatment in decrosslinking screws. The crystallinity of the decrosslinked XHDPE from TSE containing decrosslinking screws increases slightly with the ultrasonic amplitude. However, the crystallinity of decrosslinked XHDPE from TSE containing compounding screws shows a more complex behavior with a maximum at an amplitude of 5 μm. The crystallinity and melting temperature of decrosslinked XHDPE from TSE containing decrosslinking screws are higher than those from TSE containing compounding screws.

The complex behavior of the crystallinity and melting temperature of decrosslinked XHDPE seen in Figure 9 raises a question: why the rupture of the crosslink network does not always increase these values of decrosslinked XHDPE? It is natural to postulate that the rupture of the crosslink network should result in an increase of the melting temperature and crystallinity with a decrease of the gel fraction and crosslink density, owing to less restriction for lamella growth. As discussed earlier, decrosslinked XHDPE comprises the gel and sol with the sol fraction being close to or higher than the gel fraction. Hence, the effect of change of the molecular structure of the sol of decrosslinked XHDPE on the melting temperature and crystallinity of the decrosslinked XHDPE must be taken into account. In fact, as shown above, sols of decrosslinked XHDPE exhibit a higher

Table I. Cross Model Parameters and Activation Energy for Flow of the HDPE and Sols of the Decrosslinked XHDPE

Material	Amplitude, (μm)	A, (Pa*s)	T_b, (K)	τ (Pa)	n	E, (kJ/mol)
Virgin HDPE	None	0.3823	3259	3.15×10^5	0.28	27.1
Sol of Virgin XHDPE	None	0.0029	4864	6.6×10^3	0.56	40.4
	0	0.0377	6187	5.3×10^3	0.36	51.4
Sol of decrosslinked XHDPE from the	5	0.1234	6023	7.0×10^3	0.33	50.1
TSE containing compounding screws	7.5	0.0457	6234	6.5×10^3	0.35	51.8
	10	1.0113	5212	9.9×10^3	0.33	43.3
	0	0.0092	6656	1.1×10^4	0.33	55.3
Sol of decrosslinked XHDPE from the TSE containing clecrosslinking screws	5	0.0029	7258	8.0×10^3	0.36	60.3
	7.5	0.0188	6564	9.4×10^3	0.34	54.6
	10	0.0685	6640	4.6×10^3	0.30	55.2
	13	0.0431	6460	7.7×10^3	0.31	53.7

molecular weight and more chain branching than the sol of XHDPE, hindering the growth of the lamellar structure and, therefore, causing a decrease of the crystallinity and melting temperature. Accordingly, the rupture of the crosslink network of XHDPE may affect its crystallinity and melting temperature through two competing effects. The decrease of the gel fraction and crosslink density may increase the crystallinity and melting temperature of decrosslinked XHDPE, whereas the increase of sol fraction exhibiting high molecular weight and chain branching may decrease these values. As the amplitude increases, an increase in fraction of the branched sol becomes dominating effect over a decrease of the gel fraction and crosslink density. Consequently, the crystallinity and melting temperature of decrosslinked XHDPE from TSE containing compounding screws decrease at amplitudes higher than 5 μm. In case of decrosslinked XHDPE from TSE containing decrosslinking screws, a decrease of the gel fraction and crosslink density and an increase in fraction of the branched sol lead to an insignificant change in the crystallinity and melting temperature, as observed up to an amplitude of 10 μm. However, at an amplitude of 13 μm a decrease of the gel fraction and crosslink density is sufficient to induce an increase of the crystallinity in the presence of the substantial amount of the branched sol. The dependence of the crystallinity and melting temperature of decrosslinked XHDPE on screw configuration is most likely the result of a decrease of the gel fraction and crosslink density.

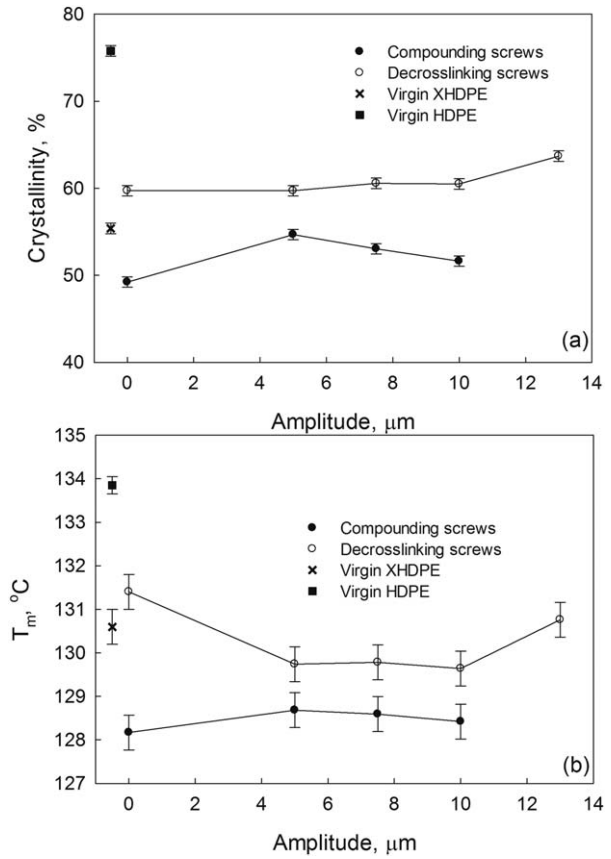

Figure 9. Crystallinity (a) and melting temperature (b) of the decrosslinked XHDPE as a function of the ultrasonic amplitude from TSE containing the compounding (filled symbols) and decrosslinking (open symbols) screws. Values of the HDPE and XHDPE are also indicated.

Morphology of the Crystalline Structure

Figure 10 shows scanning electron microscopy (SEM) images at high magnification (40,000×) on the etched cryofractured surfaces of HDPE (a), XHDPE (b), decrosslinked XHDPE at an ultrasonic amplitude of 7.5 μm from TSE containing compounding screws (c), and an ultrasonic amplitude of 13 μm from TSE containing decrosslinking screws (d). These two decrosslinked XHDPEs are chosen to examine the effect of the gel fraction on the morphology of the crystalline structure within a wide range of gel fractions. A well-developed lamellar structure is seen in Figure 10(a) owing to the linear structure of HDPE. The lamellar structure of XHDPE seen in Figure 10(b) is distorted by the presence of the crosslink network. In the presence of crosslinks, the chain folding is inhibited restricting

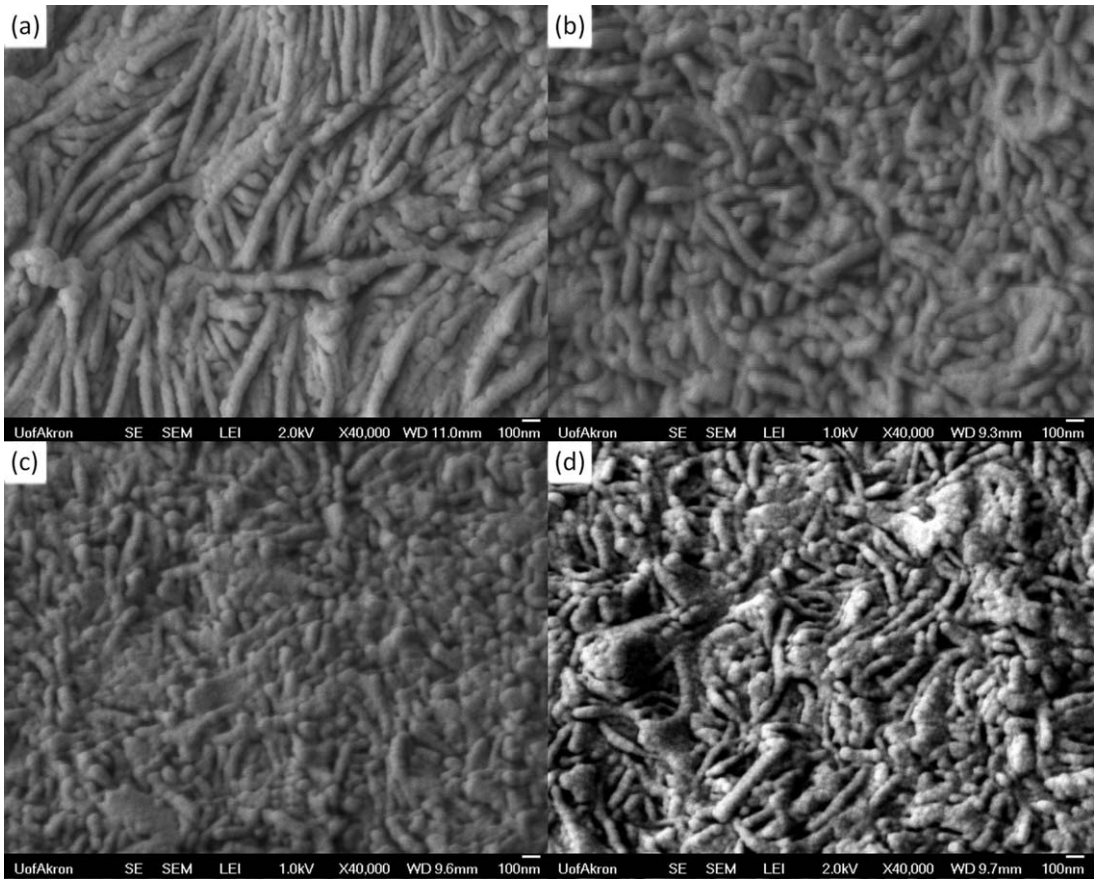

Figure 10. SEM images of the lamellar structure of the etched cryofractured surfaces of the HDPE (a), XHDPE (b), decrosslinked XHDPE at an ultrasonic amplitude of 7.5 μm from the TSE containing the compounding screws (c), and an ultrasonic amplitude of 13 μm from the TSE containing the decrosslinking screws (d). A scale bar is 100 nm.

the lamella growth in XHDPE. This observation is similar to that seen in crosslinked LDPE.[30] The lamellar structure of decrosslinked XHDPE from TSE containing compounding screws in Figure 10(c) is very similar to that of XHDPE. Although the gel fraction and crosslink density of this sample are 0.60 and 1.0×10^{-2} kmol/m^3, which indicates a substantial network rupture, these values are too high to allow growth of a well-developed lamellar structure. As seen in Figure 10(d), decrosslinked XHDPE from TSE containing decrosslinking screws, whose gel fraction is only 0.15, exhibits a well-developed lamella. Although a distortion of the lamellar structure owing to the presence of the gel is still evident, the feature of this lamellar structure is more close to that of HDPE than XHDPE. This indicates that the level of the gel fraction and crosslink density significantly affects the morphology of the lamellar structure of decrosslinked XHDPE.

Tensile Properties

Figure 11 shows the stress–strain curve of HDPE (a), decrosslinked XHDPE from TSE containing compounding screws (b), and decrosslinking screws (c) at various ultrasonic amplitudes. The stress–strain curve of XHDPE is also given in Figure 11. It is seen that the stress–strain curves of all materials exhibit the behavior of PE, i.e., yielding at low strains, necking plateau at intermediate strains, and strain hardening at high strains. Figure 12 shows the Young's modulus (a), yield stress (b), strain at break (c), and stress at break (d) of decrosslinked XHDPE as a function of the ultrasonic amplitude. The properties of HDPE and XHDPE are also indicated in the figure. It is noted that at certain amplitudes some properties of decrosslinked XHDPE from TSE containing decrosslinking screws are very close or higher to those of XHDPE. This indicates that the screw design is the key factor to obtain the decrosslinked XHDPE of superior mechanical performance.

As seen in Figure 12(a), HDPE owing to its high crystallinity exhibits a high Young's modulus. The Young's modulus of decrosslinked XHDPE obtained from TSE containing decrosslinking screws at amplitudes of 10 and 13 μm exhibits higher values than that of XHDPE and decrosslinked XHDPE obtained at other amplitudes. As no significant difference is seen between the crystallinity of decrosslinked XHDPE at various amplitudes from TSE containing decrosslinking screws, the crystallinity alone cannot explain the higher Young's modulus at amplitudes of 10 and 13 μm. Studies on the structure–tensile properties relationship of the linear[31,32] and branched[31,33] PE show that the linear PE exhibits a higher Young's modulus than the branched PE at same crystallinity. This indicates that the morphology of the crystalline structure of PE significantly influences its Young's modulus. It is known that the linear PE exhibits a

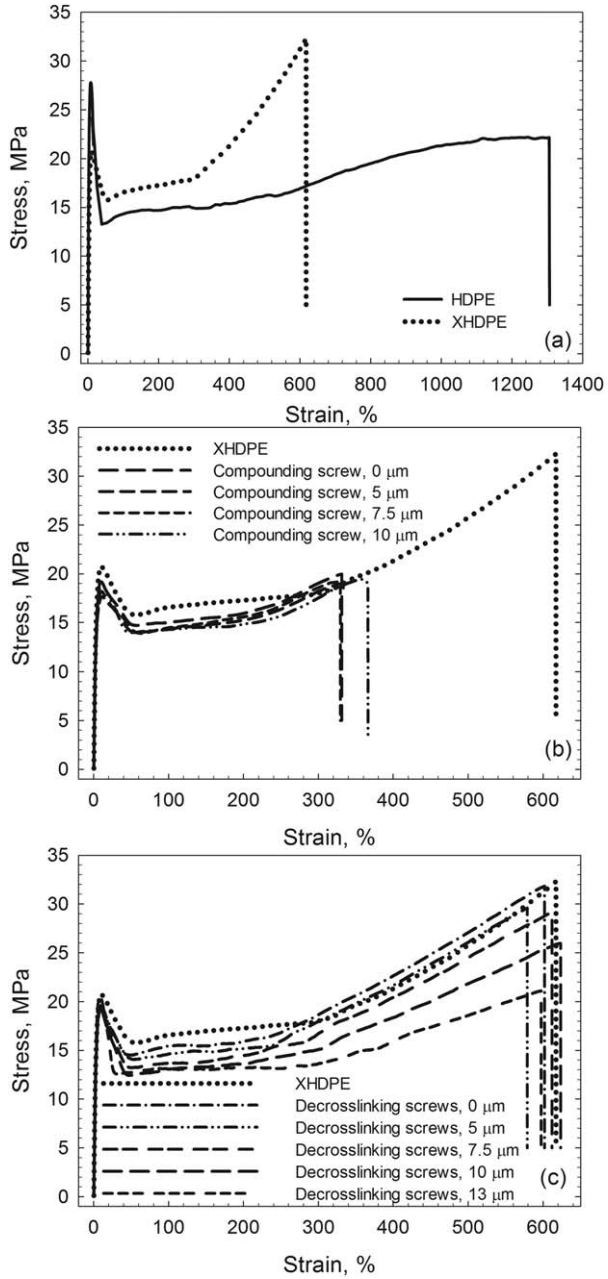

Figure 11. Stress–strain curves of HDPE (a), decrosslinked XHDPE from TSE containing compounding (b), and decrosslinking (c) screws at various ultrasonic amplitudes. The stress–strain curve of XHDPE is also indicated.

more developed lamellar structure than the branched PE with its Young's modulus being higher than that of the branched PE.[32,33] Therefore, the reason for the higher Young's modulus of these two decrosslinked XHDPE samples is most likely due to a well-developed lamellar structure.

As shown in Figure 12(b), the yield stress of HDPE owing to its higher crystallinity is higher than that of XHDPE. The yield stress of XHDPE is higher than that of decrosslinked XHDPE. The yield stress of decrosslinked XHDPE from TSE containing decrosslinking screws is higher than that from TSE containing compounding screws. This is mainly due to the fact that decrosslinked XHDPE from the former TSE exhibits a higher crystallinity than that from the latter TSE. The yield stress of decrosslinked XHDPE from TSE containing decrosslinking screws slightly increases with the ultrasonic amplitude and correlates with an increase of the crystallinity. However, the dependence of the yield stress of decrosslinked XHDPE from TSE containing compounding screws on the ultrasonic amplitude is complex and cannot be explained by the change of the crystallinity alone. The change of the crystallinity also cannot explain the fact that the yield stress of XHDPE is higher than that of decrosslinked XHDPE. It is known that the yield stress of PE is not solely depends on its crystallinity. In fact, the structure–yield stress relationship of PE is still an unresolved issue.[32–36] Extensive studies on this topic provide contradictory conclusions,[32–35] suggesting the complexity of this relationship for PE owing to its molecular structure.[33–36] Thus, the complex dependence of the yield stress of decrosslinked XHDPE from TSEs on the ultrasonic amplitude and the higher yield stress of XHDPE are results of the difference in the molecular structure.

The HDPE exhibits the highest strain at break, as seen in Figure 12(c). Again, this is due to its linear molecular structure. The strain at break of XHDPE is significantly lower than that of HDPE, because the presence of crosslinks inhibits the slippage of polymer chains during deformation. The strain at break of decrosslinked XHDPE from TSE containing decrosslinking screws is close to that of XHDPE and superior to that from TSE containing compounding screws. The superior performance of decrosslinked XHDPE from the former TSE is most likely due to a lower gel fraction and crosslink density than that from the latter TSE. Considering that the rupture of the network creates small gel clusters in decrosslinked XHDPE,[43] it is expected that the size of the gel clusters may decrease with a decrease of the gel fraction.[14] This is a natural result of the network rupture. If the stress concentration at high strains occurs at the interface between the gel and sol, it is possible that the sample containing larger gel clusters, as in the case of compounding screws, may break at a lower strain than those containing smaller gel clusters, as in the case of decrosslinking screws. This statement seems to be plausible to explain experimental observations in the present and previous study of decrosslinked XHDPE from TSE and SSE.[7] Also, it is shown that XHDPE showing strong strain hardening behavior at high strains in Figure 11 exhibits the highest stress at break [see Figure 12(d)]. HDPE owing to its weak strain hardening behavior shown in Figure 11(a) exhibits a lower stress at break than XHDPE. In fact, as the strain at break of decrosslinked XHDPE from TSE containing decrosslinking screws is close to that of XHDPE, magnitudes of the stress at break of these samples are determined by their strain hardening behavior. As seen from Figure 11(c), the strain hardening of decrosslinked XHDPE from TSE containing decrosslinking screws decreases with the ultrasonic amplitude. This is due to the fact that the strain hardening behavior increases with the crosslink density and gel fraction. Thus, the stress at break of decrosslinked XHDPE from this TSE is lower than that of XHDPE and decreases with the ultrasonic amplitude. Also, the stress at break of

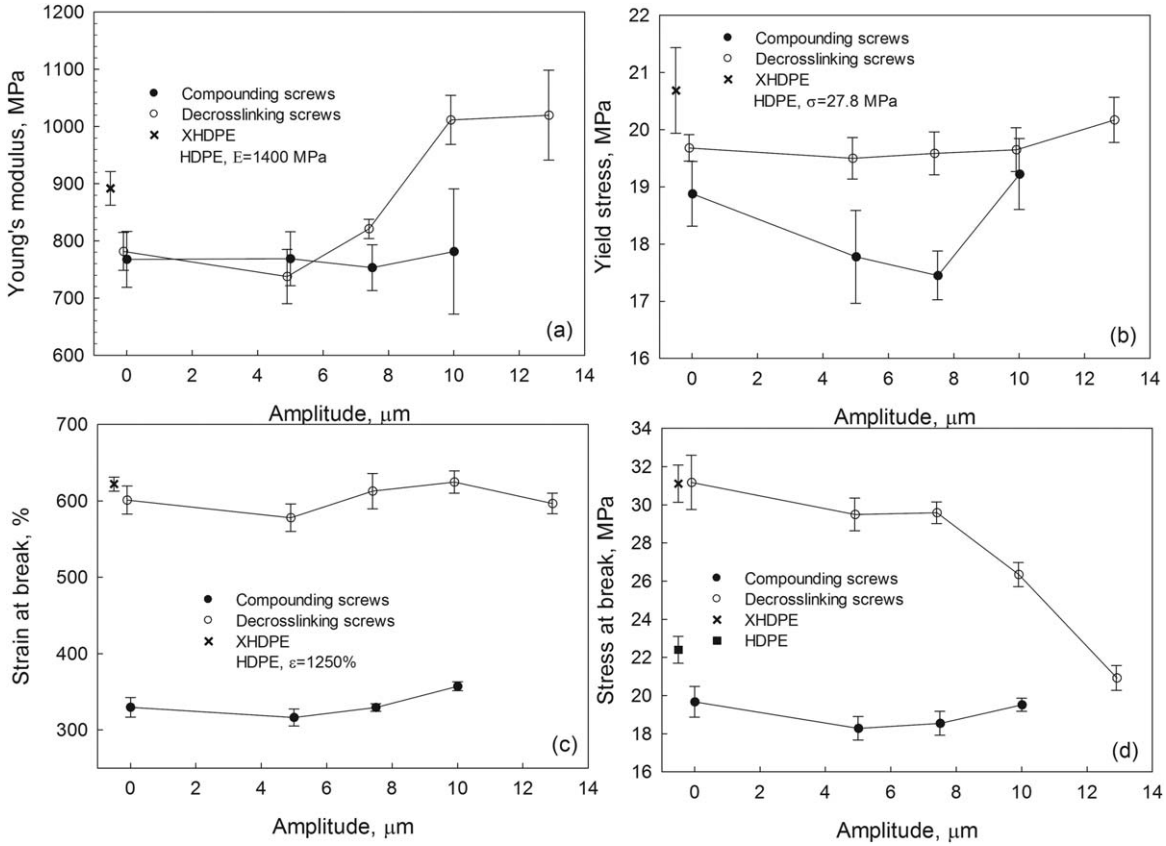

Figure 12. Young's modulus (a), yield stress (b), strain at break (c), and stress at break (d) of the decrosslinked XHDPE as a function of the ultrasonic amplitude from TSE containing compounding (filled symbols) and decrosslinking (open symbols) screws. Properties of HDPE and XHDPE are also indicated.

decrosslinked XHDPE from TSE containing decrosslinking screws without ultrasonic treatment and with ultrasonic treatment at amplitudes of 5, 7.5, and 10 μm is much higher than that from TSE containing compounding screws at same amplitudes. Because the strain at break of decrosslinked XHDPE from the former TSE is significantly higher than that of decrosslinked XHDPE from the latter TSE, decrosslinked XHDPE from the former TSE exhibits higher stress at break than those from the latter TSE.

CONCLUSIONS

Decrosslinking of XHDPE is carried out by using TSE containing decrosslinking and compounding screws without and with ultrasonic treatment at various ultrasonic amplitudes. Swelling, tensile test, and SEM are used to determine the gel fraction, crosslink density, mechanical properties, and morphology of XHDPE and decrosslinked XHDPE.

The higher efficiency of decrosslinking screws in mechanical decrosslinking is observed owing to high pressure generated by the presence of reverse conveying elements, while the higher efficiency of decrosslinking screws in ultrasonic decrosslinking is due to a higher gel fraction and crosslink density of the material entering the ultrasonic treatment zone. This is shown by numerical simulations based on a theoretical model of ultrasonic decrosslinking process. Simulations describe the effect of the residence time, gel fraction, and crosslink density of the polymer entering the ultrasonic treatment zone on structural properties of ultrasonically decrosslinked XHDPE. A fair agreement between numerical simulations and experimental observations is obtained.

Rheological properties of decrosslinked XHDPE are well correlated with the gel fraction and crosslink density. Processing–structure–rheology relationship is established. The molecular structure of sols of XHDPE and decrosslinked XHDPE is revealed by means of the SAOS test at different temperatures. The activation energies for flow of the sol of decrosslinked XHDPE and complex viscosity reveal that the sol of decrosslinked XHDPE is a highly branched PE containing long-chain branching generated by the main-chain scission during decrosslinking. The complexity of the dependence of the crystallinity and melting temperature of decrosslinked XHDPE on the ultrasonic amplitude and screw configurations is explained based on the gel fraction, crosslink density, and molecular structure of the sol.

The effect of the gel fraction on morphology of the lamellae of HDPE, XHDPE, and decrosslinked XHDPE is revealed. It is found that the presence of the gel hinders the development of the lamellar structure. By correlating the morphology with the Young's modulus of ultrasonically decrosslinked XHDPE, it is found that an increase of the Young's modulus is due to the significant change of the lamellar morphology developed in highly decrosslinked XHDPE. The mechanical performance of

decrosslinked XHDPE from TSE containing decrosslinking screws is very close to that of XHDPE and superior to decrosslinked XHDPE from TSE containing compounding screws. This study demonstrates an importance of the screw design in ultrasonic decrosslinking of XHDPE.

APPENDIX: SIMPLIFIED MODEL FOR ULTRASONIC DECROSSLINKING OF XHDPE

Under assumption that only the breakage of the main chains takes place, the normalized crosslink density of the ultrasonically decrosslinked network can be calculated as[6]:

$$\frac{v_{\text{mech+ultra}}}{v_0} = 1 - \frac{8\pi}{3^{5/2}} \frac{x_{\max}^3 - x_{\min}^3}{1 + \frac{3N}{2}} |nR_0^3 \ln (nR_0^3)| \quad \text{(A1)}$$

where $v_{\text{mech+ultra}}$ is the predicted crosslink density of ultrasonically decrosslinked XHDPE, v_0 is the crosslink density of XHDPE entering the ultrasonic treatment zone, n is the number of bubbles per unit volume, R_0 is the bubble radius at the atmospheric pressure, N is the average number of monomer units between crosslinks in the network, and $x_{\max}$ and $x_{\min}$ are, respectively, the maximum and minimum relative radius of bubble during its expansion–contraction cycle. It should be noted that eq. (A1) is only applicable for the crosslinked polymer not containing sol. Assuming that the gel is uniformly distributed in the ultrasonic treatment zone and its density equals to that of sol, eq. (A1) can be modified to take into account the effect of gel fraction into account as follows:

$$\frac{v_{\text{mech+ultra}}}{v_0} = 1 - \zeta_0 \frac{8\pi}{3^{5/2}} \frac{x_{\max}^3 - x_{\min}^3}{1 + \frac{3N}{2}} |nR_0^3 \ln (nR_0^3)| \quad \text{(A2)}$$

where ζ_0 is gel fraction of XHDPE entering the ultrasonic treatment zone. Equation (A2) calculates the normalized crosslink density of the ultrasonically decrosslinked network during one period, t, which is 2.5×10^{-5} s in the present case. The mean residence time, t_r, contains k cycles, i.e., $k = t_r/t$. Values of $v_{\text{mech+ultra}}$, $\zeta_{\text{mech+ultra}}$, $x_{\max}$, $x_{\min}$, and N are functions of time, i.e., $\zeta_{\text{mech+ultra}}$, $\zeta_{\text{mech+ultra}}(k)$, $x_{\max}(i)$, $x_{\min}(i)$, and $N(i)$, where i is the sequence of the cycle in t_r. Thus, the normalized crosslink density of the ultrasonically decrosslinked XHDPE after ultrasonic treatment for time of t_r can be expressed as:

$$\begin{aligned}\frac{v_{\text{mech+ultra}}(k)}{v_0} &= \frac{v_{\text{mech+ultra}}(1)}{v_0} \times \prod_2^k \frac{v_{\text{mech+ultra}}(i)}{v_{\text{mech+ultra}}(i-1)} \\ &= \left(1 - \zeta_0 \frac{8\pi}{3^{5/2}} \frac{x_{\max}^3(1) - x_{\min}^3(1)}{1 + \frac{3N(1)}{2}} |nR_0^3 \ln (nR_0^3)|\right) \\ &\quad \prod_2^k \left(1 - \zeta_{\text{mech+ulra}}(i) \frac{8\pi}{3^{5/2}} \frac{x_{\max}^3(i) - x_{\min}^3(i)}{1 + \frac{3N(i)}{2}} |nR_0^3 \ln (nR_0^3)|\right) \quad \text{(A3)}\end{aligned}$$

The bubble dynamics is affected by rheological properties of the decrosslinked XHDPE at an ultrasonic frequency. This frequency is within the range of the rubbery plateau of XHDPE. The effect of the crosslink network on the plateau modulus of the decrosslinked XHDPE is very small, since $M_c \gg M_e$. Therefore, the effect of network rupture on the bubble dynamics is negligible, such that the values of $x_{\max}$ and $x_{\min}$ are constants and not function of time. The value of $N(i)$ is calculated from the crosslink density as

$$N(i) = \frac{\rho}{v_{\text{mech+ultra}}(i) \times M_0} \quad \text{(A4)}$$

where M_0 is the molecular weight of ethylene. Hence, the crosslink density of the ultrasonically decrosslinked XHDPE is predicted using eqs. (A3) and (A4). In case of the rupture of the decrosslinked XHDPE due to only the main-chain scission, the gel fraction of the decrosslinked XHDPE at the end of ith period within the t_r is calculated based on the Horikx relationship describing the normalized crosslink density versus the normalized gel fraction[37]:

$$1 - \frac{v_{\text{mech+ultra}}(i)}{v_0} = 1 - \frac{(1 - (1 - \zeta_{\text{mech+ultra}}(i))^{1/2})^2}{(1 - (1 - \zeta_0)^{1/2})^2} \quad \text{(A5)}$$

Calculations based on eqs. (A3)–(A5) were done by means of an iteration scheme implemented in *MATLAB*.

To calculate the gel fraction and crosslink density, their values at the entrance of the ultrasonic treatment zone in TSE are required. Ideally, a small amount of the material can be removed from the extruder by opening the barrel after stopping the extrusion. However, this attempt was unsuccessful because the XHDPE inside the extruder experienced a noticeable chemical degradation (color change) during the disassembly. Thus, the gel fraction and the crosslink density of the material entering the ultrasonic treatment zone in TSE cannot be measured. To overcome this problem, the effect of the gel fraction of the polymer network on the ultrasonic decrosslinking of XHDPE was simulated out using several assumed values with the upper and lower limit being, respectively, the gel fraction of the XHDPE and decrosslinked XHDPE from the TSE containing the compounding screws. This was based on the following arguments. The material entering the ultrasonic treatment zone in the decrosslinking screws exhibits a higher gel fraction than that in the compounding screws. This is due to the fact that the screw elements in the decrosslinking screws in the upstream section of the cylindrical elements are all forward conveying elements generating less intensive shearing than those in the compounding screws containing kneading elements, as shown in Figure 1. Also, the gel fraction of the material entering the ultrasonic treatment zone in the compounding screws is higher than the gel fraction of the decrosslinked XHDPE from the same TSE without ultrasonic treatment. Thus, the value of the gel fraction was varied from 0.805 for the XHDPE to 0.625 for the decrosslinked XHDPE from the compounding screws without ultrasonic treatment. The corresponding values of the crosslink density of the material entering the ultrasonic treatment zone in TSE are calculated based on eq. (A5).

To calculate the gel fraction and crosslink density, the values of n and R_0 in eq. (2) were assigned to be similar for both TSEs. The values of $x_{\max}$ and $x_{\min}$ were calculated according to the procedures reported in Ref. 8. The bubble dynamics is calculated by solving the equation of motion by considering the XHDPE as a viscoelastic solid with one relaxation mode. The model requires the storage modulus in the rubbery and glassy states and loss tangent at the ultrasonic frequency. The storage

Table AI. Parameters and Material Constants Used in Simulation of the Decrosslinking of XHDPE in TSE with Two Screw Configurations

Description	XHDPE	Reference source
Density, kg/m^3	730	29
Surface tension, N/m	0.028	40
Shear modulus at ω=0, MPa	2.6	41
Shear modulus at $\omega = \infty$, MPa	856	Measured value
Loss tangent at 40 kHz	0.03	39
Bulk sound velocity, m/s	1000	42
Initial bubble radius, μm	30	As signed value
Bubble concentration, m^{-3}	2 x 10^{11}	Assigned Value
Hydrostatic pressure, MPa	0.4	Assigned Value

modulus of the XHDPE measured in the oscillatory tension (not reported here) below its glass transition temperature is obtained. The shear storage modulus in the glassy state was calculated using Poisson ratio of 0.46 of the HDPE.[38] As the ultrasonic frequency is within the rubbery plateau, the plateau modulus (G_N^0) of the linear PE is taken as the shear modulus in the rubbery state. It should be noted that the value of G_N^0 cannot be obtained directly or using the frequency-temperature superposition, because the ultrasonic frequency used is three orders of magnitude higher than the upper limit of the frequency in the SAOS test. Also, the loss tangent of the XHDPE at 200°C at the ultrasonic frequency cannot be measured in the SAOS test. Fortunately, the loss tangent of the molten LLDPE at the frequency of 2×10^4 rad/s was measured by a piezoelectric rotary vibrator.[39] The extrapolation of the dynamic moduli of this particular LLDPE indicated that the loss tangent at the frequency of 10^5 rad/s is about 0.03 at 150°C. As the ultrasonic frequency used in our study is 2.5×10^5 rad/s, the extrapolated value of the loss tangent of LLDPE at the frequency of 10^5 rad/s is used in calculations. All the parameters and material constants used in simulations are tabulated in Table AI.

ACKNOWLEDGMENTS

Financial support for this work by NSF grant no. CMMI-1131342 is greatly appreciated. The authors thank the Exxon Mobil Chemical Company for providing HDPE and the Akrochem Corporation for providing peroxide. They also thank Mr. Todd M. Lewis for the fruitful discussion on the screw design.

REFERENCES

1. Goto, T.; Yamazaki, T.; Sugeta, T.; Okajima, I.; Sako, T. *J. Appl. Polym. Sci.* **2008**, *109*, 144.
2. Lee, H.-s.; Jeong, J. H.; Hong, G.; Cho, H.-K.; Baek, B. K.; Koo, C. M.; Hong, S. M.; Kim, J.; Lee, Y.-W. *Ind. Eng. Chem. Res.* **2013**, *52*, 6633.
3. Isayev, A. I.; Ghose, S. In Rubber Recycling; De, S. K., Isayev, A. I., Khait, K., Eds.; CRC Press: Boca Raton, FL, **2005**; Chapter *9*, p 311.
4. Isayev, A. I. In Science and Technology of Rubber, 3rd ed.; Mark, J. E., Erman, B., Eirich, F. R., Eds.; Academic Press: New York, **2005**; Chapter *15*, p 663.
5. Isayev, A. I.; Jenkins, J. *SPE ANTEC Tech. Pap.* **2008**, *53*, 109.
6. Yashin, V. V.; Isayev, A. I. *Rubber Chem. Technol.* **2000**, *73*, 325.
7. Huang, K.; Isayev, A. I. SPE ANTEC Technical Papers **2013**, *58*, 972.
8. Yashin, V. V.; Isayev, A. I. *Rubber Chem. Technol.* **1999**, *72*, 741.
9. Crawford, R. J.; Throne, J. L. Rotational Molding Technology; William Andrew Publishing: New York, **2002**; p 24.
10. Flory, P. J. *J. Chem. Phys.* **1950**, *18*, 108.
11. Ng, T. S. K.; McKinley, G. H. *J. Rheol.* **2008**, *52*, 417.
12. Zhu, L.; Chiu, F.; Fu, Q.; Quirk, R. P.; Cheng, S. Z. D. Polymer Handbook, 4th ed.; Wiley, **1999**; p V–17.
13. Olley, R. H.; Basset, D. C. *Polymer* **1982**, *23*, 1707.
14. Venkataraman, S. K.; Winter, H. H. *Rheol. Acta* **1990**, *29*, 423.
15. Hatzikriakos, S. G.; Dealy, J. M. *J. Rheol.* **1992**, *36*, 703.
16. Hong, C. K.; Isayev, A. I. *Elastomer* **2003**, *38*, 103.
17. Winter, H. H.; Chambon, F. *J. Rheol.* **1986**, *30*, 367.
18. Vallés, E. M.; Carella, J. M.; Winter, H. H.; Baumgaertel, M. *Rheol. Acta* **1990**, *29*, 535.
19. Chambon, F.; Winter, H. H. *J. Rheol.* **1987**, *31*, 683.
20. Yamaguchi, M.; Suzuki, K.-I.; Maeda, S. *J. Appl. Polym. Sci.* **2002**, *86*, 73.
21. Zhang, X.; Yang, H.; Song, Y.; Zheng, Q. *Polymer* **2012**, *53*, 3035.
22. Stadler, F. J.; Piel, C.; Kaschta, J.; Rulhoff, S.; Kaminsky, W.; Münstedt, H. *Rheol. Acta* **2006**, *45*, 755.
23. Lohse, D.; Milner, S.; Fetters, L.; Xenidou, M.; Hadjichristidis, N.; Mendelson, R.; Garcia-Franco, C.; Lyon, M. *Macromolecules* **2002**, *35*, 3066.
24. Raju, V.; Smith, G.; Marin, G.; Knox, J.; Graessley, W. *J. Polym. Sci. Polym. Phys. Ed.* **1979**, *17*, 1183.
25. Rochefort, W.; Smith, G.; Rachapudy, H.; Raju, V.; Graessley, W. *J. Polym. Sci. Polym. Phys. Ed.* **1979**, *17*, 1197.
26. Raju, V.; Rachapudy, H.; Graessley, W. *J. Polym. Sci. Polym. Phys. Ed.* **1979**, *17*, 1223.
27. Pearson, D.; Ver Strate, G.; Von Meerwall, E. D.; Schilling, F. *Macromolecules* **1987**, *20*, 1133.
28. Cross, M. M. *Rheol. Acta* **1979**, *18*, 609.
29. Mavridis, H.; Shroff, R. *Polym. Eng. Sci.* **1992**, *32*, 1778.
30. Gohil, R. M.; Phillips, P. *J. Polymer* **1986**, *26*, 1687.
31. Popli, R.; Mandelkern, L. *J. Polym. Sci. Part B: Polym. Phys.* **1987**, *25*, 441.
32. Kennedy, M. A.; Peacock, A. J.; Mandelkern, L. *Macromolecules* **1994**, *27*, 5297.
33. Kennedy, M. A.; Peacock, A. J.; Failla, M. D.; Lucas, J. C.; Mandelkern, L. *Macromolecules* **1995**, *28*, 1407.
34. Humbert, S.; Lame, O.; Vigier, G. *Polymer* **2009**, *50*, 3755.

35. Darras, O.; Séguéla, R. *J. Polym. Sci. Part B: Polym. Phys.* **1993**, *31*, 759.
36. Gaucher-Miri, V.; Séguéla, R. *Macromolecules* **1997**, *30*, 1158.
37. Horikx, M. M. *J. Polym. Sci.* **1956**, *19*, 445.
38. Bédoui, F.; Diani, J.; Régnier, G. *Polymer* **2004**, *45*, 2433.
39. Chen, X.; Stadler, F. J.; Münstedt, H.; Larson, R. G. *J. Rheol.* **2010**, *53*, 393.
40. Roe, R. J. *J. Phys. Chem.* **1968**, *72*, 2013.
41. Fetters, L. J.; Lohse, D. J.; Richter, D.; Witten, T. A.; Zirkel, A. *Macromolecules* **1994**, *27*, 4639.
42. Gendron, R.; Taibouet, J.; Guevremont, J.; Dumoulin, M.; Piché, L. *Polym. Eng. Sci.* **1995**, *35*, 79.
43. Isayev, A. I.; Huang, K. *Polym. Eng. Sci.* doi: 10.1002/pen.23827 (early view, 2013).